Chapter 6

FLOOR FAILURE ANALYSIS AT LONGWALL MINING FACE BASED ON THE MULTIPLE SLIDING BLOCK MODEL

6.1 INTRODUCTION

This chapter presents an analytical model of floor failure mechanism at a longwall coal mining face based on a multiple sliding block model. During longwall mining, stresses and displacements of strata are constantly changing. High stress concentrations can exceed rock strength and initiate strata fractures that can, under unfavourable conditions, lead to large floor displacements and disruption of mining.

Underground observations of the rock floor and computational modelling of the longwall face, indicate that sub-vertical fractures and bedding plane shear dominates floor failure. Extensive lateral shearing of weak bedding planes typically present in the sedimentary strata and sub-vertical fractures that usually occur at regular intervals during face advance give, the floor strata a typical blocky appearance.

Fractures that develop ahead of the longwall face are subject to a 'secondary' movement when exposed ahead of the longwall supports. As coal is mined from above, floor strata moves toward the opening, causing the floor to bend. If the floor fails, blocks displace in response to floor movement and interact at the fractured surfaces. The analysis described in this chapter attempts to explain how stress distribution that develops within broken floors during an active movement of floor strata leads to high stress concentrations at floor level. These stress concentrations can exceed rock strength and induce compression failure of the floor that may interfere with longwall operations.

The multiple sliding block geometry within the floor was developed on the basis of observations presented in Chapter 3, while the analytical formulations presented here are supplemented by numerical modelling to verify that the results are in accordance with numerical predictions.

6.2 PROPOSED MECHANISM FOR THE MULTIPLE SLIDING BLOCK MODEL

The proposed floor failure mechanism based on a multiple sliding block model can develop where geological conditions are favourable (Terzaghi, 1967). These conditions require extensive lateral fracturing that often develop along the numerous weak bedding planes present in sedimentary strata, and sub-vertical fractures that normally form in response to changing stress abutments ahead of the longwall coal face. These failure mechanisms were extensively

modelled (Gale, 1998) and measured underground using microseismic surveys (Kelly, 1998). Lateral and near vertical fracture planes that define stone blocks within the mining floor will interact during floor heave and can induce large stresses at the corners of the blocks.

The analytical solution for multiple sliding blocks was specifically designed to suit floor movement. The analysis assumes a failed bedding plane deep within the floor and near vertical fractures forming at regular intervals that define the geometry of moving blocks (Nemcik, 1998). It also assumes planar and curved floor inclinations on which the blocks move. Progressive floor uplift (Peng, 1984) and the reaction forces generated at the face initiate block movement while continuous floor uplift creates an inclined surface on which the blocks can slide. Analytical equations have been derived to calculate stress magnitudes at the block corners during floor uplift and describe the force generated between free-standing blocks with an additional loading of powered supports.

The computational model was formulated to compare analytical solutions with the numerical results and simulate the interaction of blocks standing on an inclined floor experiencing uplift. This simulation was repeated for a number of planar and parabolic floor inclinations including an additional vertical loading induced by powered supports.

6.3 POST FAILURE BEHAVIOUR OF FLOOR SPLIT BY MINING INDUCED FRACTURES

The following analysis assumes that a single bedding plane fails below the floor and that vertical fractures develop ahead of the longwall face at regular intervals forming blocks, as shown in Figure 6.1. Progressive longwall mining causes continuous floor uplift at the longwall face which initiate an active slip of blocks along the sub-vertical fractures and lateral slip along the failed bedding plane.

The analytical approach and numerical modelling are presented to explain how continuous floor deformation and actively sliding blocks can induce lateral stress concentrations at the floor level. Block behaviour varies according to geometry and angle of friction along the slip surfaces. In most cases, near vertical fracture surfaces dip steeply towards the goaf so vertical surfaces were assumed to simplify calculation of forces at the block sides.

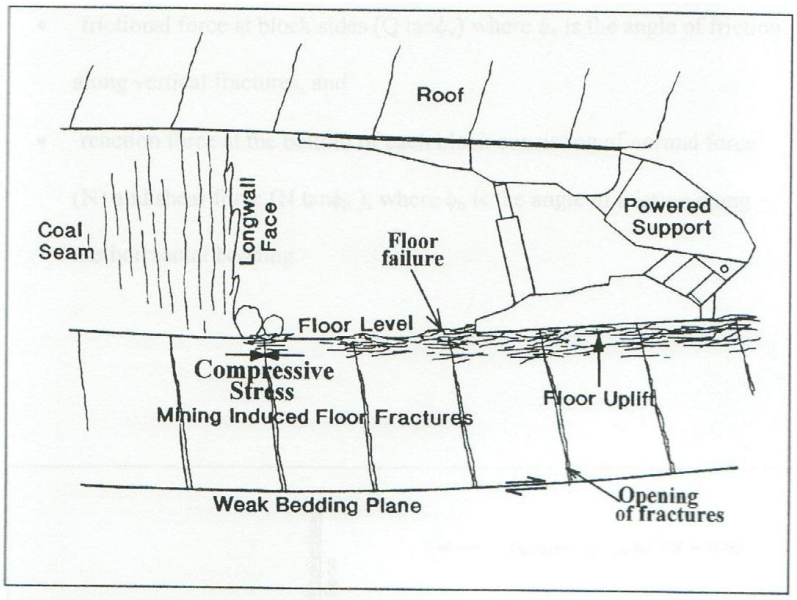

Figure 6.1 Floor fractures and floor uplift at longwall face

6.4 ACTIVE SLIP OF BLOCKS RESTING ON AN INCLINED BEDDING PLANE

In response to longwall mining, continuous floor uplift is generally experienced as illustrated in Figure 6.2 while Figure 6.3 describes forces of actively slipping blocks standing on an inclined surface subject to:

- weight of block (W)
- lateral interaction force (Q)

- frictional force at block sides (Q $\tan\phi_v$) where ϕ_v is the angle of friction along vertical fractures, and
- reaction force at the bottom of each block consisting of normal force (N) and shear force (N $\tan\phi_h$), where ϕ_h is the angle of friction along the horizontal bedding.

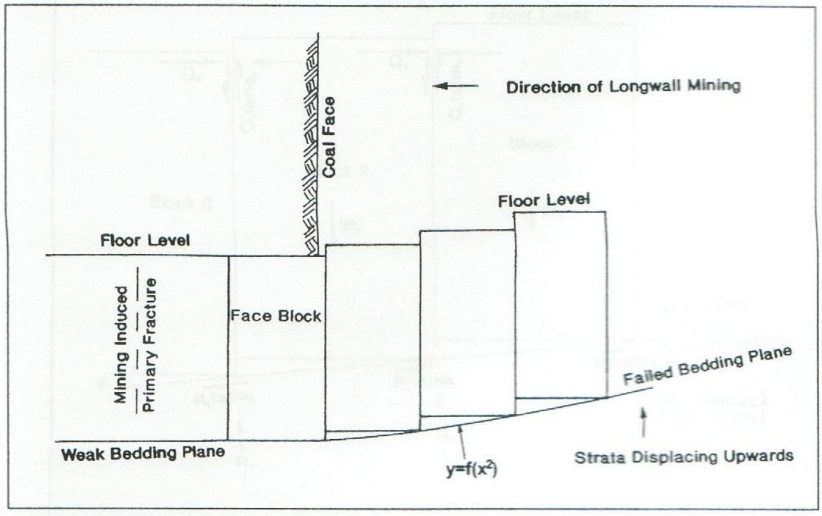

Figure 6.2 Schematic representation of block movement in floor

Note that the blocks move upwards, that the shear forces along the sides of the blocks are also in the direction of movement and the friction along vertical fractures increases with the normal force N_i at the base of each block. The ability to slip either along the vertical plane or the horizontal bedding appears

to be related to floor shape, block geometry and the angle of friction along the slip surfaces.

Three possible cases of block behaviour are shown in Figure 6.4, with each case being described and analysed in the following pages.

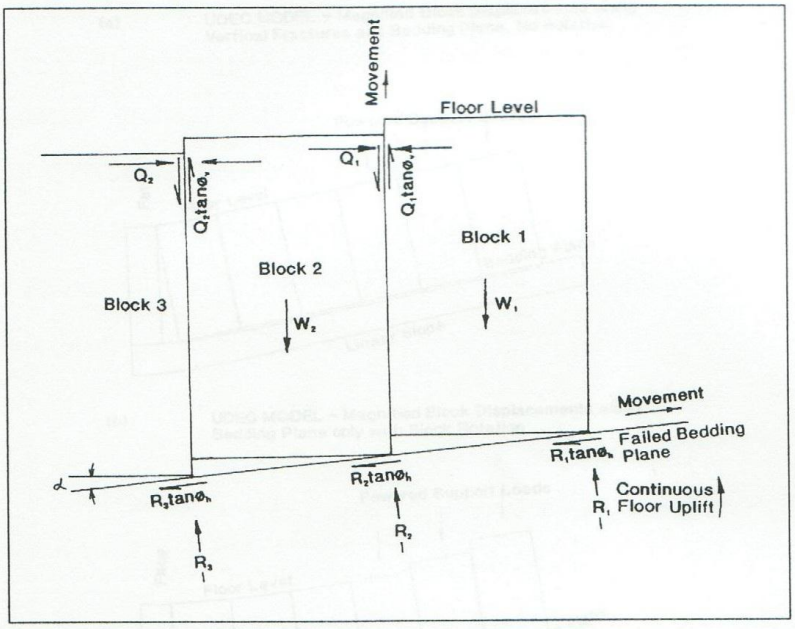

Figure 6.3 Schematic representation of acting forces on block sides experiencing floor tilt

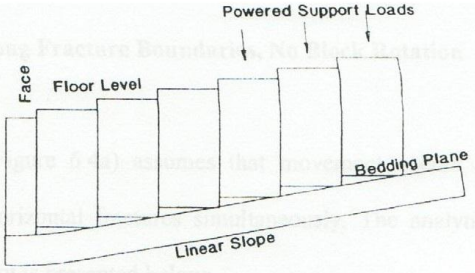

(a) UDEC MODEL - Magnified Block Displacements along Vertical Fractures and Bedding Plane, No Rotation

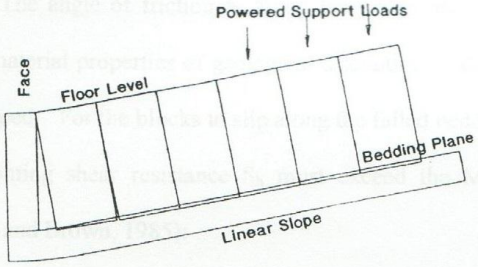

(b) UDEC MODEL - Magnified Block Displacements along Bedding Plane only with Block Rotation

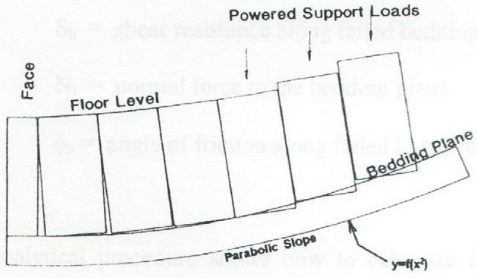

(c) UDEC MODEL - Magnified Block Displacements along Bedding Plane with Complex Block Rotation

Figure 6.4 UDEC model of magnified block displacements

6.4.1 Slip Along Fracture Boundaries, No Block Rotation

This model (Figure 6.4a) assumes that movement occurs along both the vertical and horizontal fractures simultaneously. The analytical solution of block movement is presented below:

A free body diagram presented in Figure 6.3 shows the forces acting upon a single block. The angle of friction ϕ_h along the failed bedding plane will depend on the material properties of geological discontinuity along which the failure is developed. For the blocks to slip along the failed bedding plane, the force F_s overcoming shear resistance S_h must exceed the Mohr-Coulomb criterion (Brady and Brown, 1985):

$$F_s > S_h \text{ , and}$$

$$S_h = N_i \tan\phi_h$$

where, S_h = shear resistance along failed bedding plane

N_i = normal force to the bedding plane

ϕ_h = angle of friction along failed horizontal bedding

The following analytical procedure shows how to calculate the maximum lateral force Q concentrated at the point of contact at the top corner of each block resting on an inclined surface.

In order to derive an equation to evaluate Q forces at block corners, the first trial assumes that floor surface inclination α is planar, includes self-weight of

the floor and the additional surface load P. Consider the "block$_1$" at the edge of the boundary as shown in Figure 6.4.

From the free body diagram in Figure 6.3 it can be observed that the normal force to the bedding plane at the block$_1$ is given by:

$$N_1 = W_1\cos\alpha + \tan\phi_v Q_1\cos\alpha + \sin\alpha Q_1 \qquad (6.1)$$

The normal force to the bedding plane N_2 at the block$_2$ is:

$$N_2 = W_2\cos\alpha + \tan\phi_v (Q_2 - Q_1)\cos\alpha + \sin\alpha(Q_2 - Q_1) \qquad (6.2)$$

Similarly it can be derived that the normal force at block$_i$ is:

$$N_i = W_i\cos\alpha + \tan\phi_v (Q_i - Q_{i-1})\cos\alpha + \sin\alpha(Q_i - Q_{i-1}) \qquad (6.3)$$

The lateral force Q_1 is equal to:

$$Q_1 = N_1(\sin\alpha + \tan\phi_h\cos\alpha) \qquad (6.4)$$

Substituting Equation (6.1) for N_1 leads to:

$$Q_1 = (W_1\cos\alpha + \tan\phi_v\cos\alpha Q_1 + \sin\alpha Q_1)(\sin\alpha + \tan\phi_h\cos\alpha)$$

Solving for Q_1,

$$Q_1 = \frac{W_1 \cos\alpha(\sin\alpha + \tan\phi_h \cos\alpha)}{1 - (\tan\phi_v \cos\alpha + \sin\alpha)(\sin\alpha + \tan\phi_h \cos\alpha)}$$

Rearranging gives:

$$Q_1 = \frac{W_1 \cos\alpha}{(\sin\alpha + \tan\phi_h \cos\alpha)^{-1} - (\sin\alpha + \tan\phi_v \cos\alpha)} \tag{6.5}$$

The lateral force Q_2 is equal to:

$$Q_2 = (N_1 + N_2)(\sin\alpha + \tan\phi_h \cos\alpha) \tag{6.6}$$

Substituting Equations (6.1) and (6.2) for N_1 and N_2 gives:

$$Q_2 = (W_1 \cos\alpha + \tan\phi_v \cos\alpha Q_1 + \sin\alpha Q_1 + W_2 \cos\alpha + \tan\phi_v \cos\alpha Q_2 - \\ - \tan\phi_v \cos\alpha Q_1 + \sin\alpha Q_2 - \sin\alpha Q_1)(\sin\alpha + \tan\phi_h \cos\alpha)$$

Simplifying the above leads to:

$$Q_2 = (W_1 \cos\alpha + W_2 \cos\alpha + \tan\phi_v \cos\alpha Q_2 + \sin\alpha Q_2)(\sin\alpha + \tan\phi_h \cos\alpha)$$

Solving for Q_2 gives:

$$Q_2 = \frac{(W_1 + W_2)\cos\alpha(\sin\alpha + \tan\phi_h \cos\alpha)}{1-(\sin\alpha + \tan\phi_v \cos\alpha)(\sin\alpha + \tan\phi_h \cos\alpha)} \qquad \text{or}$$

$$Q_2 = \frac{(W_1 + W_2)\cos\alpha}{(\sin\alpha + \tan\phi_h \cos\alpha)^{-1} - (\sin\alpha + \tan\phi_v \cos\alpha)} \tag{6.7}$$

Further it can be proven that for any force Q_n:

$$Q_n = \frac{\sum_{i=1}^{n} W_i \cos\alpha}{(\sin\alpha + \tan\phi_h \cos\alpha)^{-1} - (\sin\alpha + \tan\phi_v \cos\alpha)} \tag{6.8}$$

For the blocks of the same weight, the equation is linear and becomes

$$Q_n = \frac{nW\cos\alpha}{(\sin\alpha + \tan\phi_h \cos\alpha)^{-1} - (\sin\alpha + \tan\phi_v \cos\alpha)} \tag{6.9}$$

Expanding Equation (6.9) gives:

$$Q_n = \frac{nW(\sin\alpha\cos\alpha + \tan\phi_v \cos^2\alpha)}{1-\tan\phi_v \sin\alpha\cos\alpha + \sin^2\alpha - \tan\phi_h \tan\phi_v \cos^2\alpha + \tan\phi_h \sin\alpha\cos\alpha} \tag{6.10}$$

If the inclined slope on which the blocks slide is not planar and

$$\alpha_i \neq \alpha_{i-1} \neq \alpha_{i-2} \neq \ldots\ldots \alpha_1,$$

Q force can be calculated as shown below:

$$Q_1 = \frac{W_1 \cos\alpha_1}{(\sin\alpha_1 + \tan\phi_h \cos\alpha_1)^{-1} - (\sin\alpha_1 + \tan\phi_v \cos\alpha_1)} \quad (6.11)$$

The Q_2 is dependent on Q_1 and becomes:

$$Q_2 = \frac{W_2 \cos\alpha_2 - Q_1\{(\sin\alpha_2 + \tan\phi_v \cos\alpha_2) - (\sin\alpha_2 + \tan\phi_h \cos\alpha_2)^{-1})}{(\sin\alpha_2 + \tan\phi_h \cos\alpha_2)^{-1} - (\sin\alpha_2 + \tan\phi_v \cos\alpha_2)} \quad (6.12)$$

and for any force Q_n, it can be proven that:

$$Q_n = \sum_{i=1}^{n} \frac{W_i \cos\alpha_i - Q_{i-1}\{(\sin\alpha_i + \tan\phi_v \cos\alpha_i) - (\sin\alpha_i + \tan\phi_h \cos\alpha_i)^{-1}\}}{(\sin\alpha_i + \tan\phi_h \cos\alpha_i)^{-1} - (\sin\alpha_i + \tan\phi_v \cos\alpha_i)} \quad (6.13)$$

6.4.2 Height of the Lateral Force Centroid Q_i

Assuming that $W_1 = W_2 = W_{3....} = W$ and $\alpha_1 = \alpha_2 = \alpha_3 = ... \alpha$

Taking moments about the normal force interaction point N_1 of the first block$_1$:

$$\frac{WL}{2} - Q_1 h_1 + LQ_1 \tan\phi_v = 0 \qquad (6.14)$$

Solving for the height of centroid h_1 gives:

$$h_1 = \frac{WL}{2Q_1} + L\tan\phi_v \qquad (6.15)$$

Substituting Equation (6.5) for Q_1 gives:

$$h_1 = \frac{L\{(\sin\alpha + \tan\phi_h \cos\alpha)^{-1} - (\sin\alpha + \tan\phi_v \cos\alpha)\}}{2\cos\alpha} + L\tan\phi_v \qquad (6.16)$$

Similarly taking moments about the normal force point N_2 of the block$_2$:

$$\frac{WL}{2} - Q_1 h_1 + LQ_2 \tan\phi_v - Q_2 h_2 = 0 \qquad (6.17)$$

Solving for h_2:

$$h_2 = \frac{WL}{2Q_2} + L\tan\phi_v + h_1 \frac{Q_1}{Q_2} \qquad (6.18)$$

Substituting Equation (6.5), (6.7) and (6.15) for Q_1, Q_2 and h_1 leads to:

$$h_2 = \frac{L\{(\sin\alpha + \tan\phi_h \cos\alpha)^{-1} - (\sin\alpha + \tan\phi_v \cos\alpha)\}}{2\cos\alpha} + \frac{3L\tan\phi_v}{2} \qquad (6.19)$$

Similarly it can be proven that:

$$h_i = \frac{L\{(\sin\alpha + \tan\phi_h \cos\alpha)^{-1} - (\sin\alpha + \tan\phi_v \cos\alpha)\}}{2\cos\alpha} + \frac{(i+1)L\tan\phi_v}{2} \qquad (6.20)$$

Equation (6.20) indicates that as the distance from the block$_1$ increases (term i+1), the height of the centroid Q_i increases until it coincides with the top corner of the block, where $h_i = H_i$.

The condition of the block rotation can be described as:

$$Q_{i+1}(h_{i+1} - \frac{H}{2}) + \frac{N_i H}{2}\tan\phi_h < (Q_{i+1} + Q_i)\frac{L}{2}\tan\phi_v + \frac{N_i L}{2} + Q_i(h_i - \frac{H}{2}) \qquad (6.21)$$

If the left hand side of the Equation (6.21) is smaller than the right hand side, the block will rotate to the position where the base is in full contact with the bedding plane. Equation (6.21) indicates that if the angle of friction along the bedding plane decreases while the friction angle along the vertical fractures increases, the chance of block rotation will increase. Reducing the geometrical ratio H/L would also increase the likelihood of block rotation.

6.4.3 Additional Load induced by Powered Supports

An additional load P_i induced on the block$_i$ by the powered supports modifies the above equations as given below where Equation (6.3) is modified to:

$$N_i = (W_i+P_i)\cos\alpha + \tan\phi_v\cos\alpha\,(Q_i-Q_{i-1})+ \sin\alpha(Q_i-Q_{i-1}) \qquad (6.22)$$

where, P_i = Load of Powered support on block$_i$

Equation (6.9), (6.13) and (6.20) now become:

$$Q_n = \frac{n(W+P)\cos\alpha}{(\sin\alpha+\tan\phi_h\cos\alpha)^{-1}-(\sin\alpha+\tan\phi_v\cos\alpha)} \qquad (6.23)$$

$$Q_n = \sum_{i=1}^{n}\frac{(W_i+P_i)\cos\alpha_i - Q_{i-1}\{(\tan\phi_v\cos\alpha_i+\sin\alpha_i)-(\sin\alpha_i+\tan\phi_h\cos\alpha_i)^{-1}\}}{(\sin\alpha_i+\tan\phi_h\cos\alpha_i)^{-1}-(\sin\alpha_i+\tan\phi_v\cos\alpha_i)} \qquad (6.24)$$

$$h_i = \frac{L(P_i+\frac{W_i}{2})\{(\sin\alpha+\tan\phi_h\cos\alpha)^{-1}-(\sin\alpha+\tan\phi_v\cos\alpha)\}}{(P_i+W_i)2\cos\alpha}+\frac{(i+1)L\tan\phi_v}{2} \qquad (6.25)$$

Equation 6.25 indicates that the Q forces are largest at the longwall face and the P force induced by powered supports increases the Q forces significantly.

6.4.4 Rotation of Block with Slip along the Bedding Plane

The Equation (6.20) indicates that the centroid h_i of the lateral force Q_i is sensitive to the friction angle along the vertical fractures, and the distance towards the face. The friction angle along the vertical fractures ϕ_V is typically $\approx$35° and possibly higher due to an uneven fracture surface (angle i). Under the conditions described by Equation (6.23), rotation will occur and the base of the block will move to the position shown earlier in Figure 6.4(b). The analytical solution and the computational model indicate that if block rotation occurs during active block movement, normal stress at the base is, in most cases, concentrated close to the uphill corner of each block. For block rotation, the lateral force Q can be calculated as described in the following section.

6.4.5 Rotation of Block with No Slip along Vertical Fractures

For planar bedding inclination α (Figure 6.4b), calculations of the Q_n force at the coal face can be determined as follows. The Q forces are taken as being parallel to the bedding plane. Taking moments about the face point where the Q_n force is calculated and considering all "n" blocks at once, the sum of forces is equal to zero. Therefore,

$$\sum_{i=1}^{n}\{(W_i + P_i)(n-i+1/2)L + N_i(H\tan\phi_h - 1)\} = 0 \qquad (6.26)$$

where, L = width of the blocks

H = height of the blocks

Solving for the sum of normal forces N_i :

$$\sum_{i=1}^{n} N_i = \sum_{i=1}^{n}\{(1 - H\tan\phi_h) - (W_i + P_i)(n-i+1/2)L\} \qquad (6.27)$$

Finally, the Q_n force can be calculated as shown below:

$$Q_n = \sum_{i=1}^{n} N_i \tan\phi_h \qquad (6.28)$$

6.4.6 Rotation of Block with No Slip along Vertical Fractures standing on a Curved Slope

For curved bedding inclination as shown in Figure 6.4c, Q forces were taken as being parallel to the bedding plane. By taking moments about the top left corner of each block where the Q forces are transferred through, the normal force at the base of $block_1$ is equal to:

$$N_1 = \frac{0.5L(W_1 + P_1)}{L - H\tan\phi_h} \tag{6.29}$$

Summing the forces parallel to the bedding plane, the Q_1 force can be calculated as:

$$Q_1 = N_1 \tan\phi_h \tag{6.30a}$$

Substituting for N_1 :

$$Q_1 = \frac{0.5L(W_1 + P_1)}{L - H\tan\phi_h}\tan\phi_h \tag{6.30b}$$

Similarly for $block_2$:

$$N_2 = \frac{0.5L(W_2 + P_2) - LV_1\cos(\alpha_1 - \alpha_2)}{L - H\tan\phi_h} \tag{6.31}$$

where, V_1 is the force along the vertical fracture of $Block_1$ and is equal to:

$$V_1 = N_1 - (W_1 + P_1) \tag{6.32}$$

Summing the forces parallel to the bedding plane, the Q_2 force can be calculated as:

$$Q_2 = N_2 \tan\phi_h + Q_1\cos(\alpha_1 - \alpha_2) \tag{6.33}$$

Substituting for N_2 :

$$Q_2 = \frac{0.5L(W_2 + P_2) - \mathrm{LV}_1 \cos(\alpha_1 - \alpha_2)}{L - H \tan\phi_h} \tan\phi_h + Q_1 \cos(\alpha_1 - \alpha_2) \qquad (6.34)$$

It can be derived that for any term N_i:

$$N_i = \frac{0.5L(W_i + P_i) - \mathrm{LV}_{i-1} \cos(\alpha_i - \alpha_{i-1})}{L - H \tan\phi_h} \qquad (6.35)$$

V_{i-1} is the frictional force along the vertical fracture on the right side of block$_i$ and must be smaller than $Q_i \tan\phi_v$. Any frictional force along the vertical fracture can be iterated by:

$$V_i = V_{i-1} + N_i - W_i - P_i \qquad (6.36)$$

The general Q force can be evaluated as:

$$Q_i = N_i \tan\phi_h + Q_{i-1} \cos(\alpha_i - \alpha_{i-1}) \qquad \text{or} \qquad (6.37)$$

$$Q_i = \frac{0.5L(W_i + P_i) - \mathrm{LV}_{i-1} \cos(\alpha_i - \alpha_{i-1})}{L - H \tan\phi_h} \tan\phi_h + Q_{i-1} \cos(\alpha_i - \alpha_{i-1}) \qquad (6.38)$$

6.4.7 Rotation of Block with Slip along Vertical Fractures

For certain conditions along the non-planar bedding inclination α_i as shown in Figure 6.4 (c), the slip along the vertical fractures will occur. In this case, the Q forces are taken as being parallel to the bedding plane.

Summing the forces perpendicular to the bedding plane, the normal force to the bedding at $Block_1$ can be calculated by:

$$N_1 = (W_1+P_1)\cos\alpha_1 + Q_1\tan\phi_v \tag{6.39}$$

Summing the forces parallel to the bedding plane, the Q_1 force can be evaluated to give:

$$Q_1 = N_1\tan\phi_h + (W_1+P_1)\sin\alpha_1 \tag{6.40}$$

Substituting for N_1 and rearranging gives:

$$Q_1 = \frac{(W_1 + P_1)(\sin\alpha_1 + \tan\phi_h\cos\alpha_1)}{1 - \tan\phi_h \tan\phi_v} \tag{6.41}$$

Similarly for $block_2$:

$$N_2 = (W_2+P_2)\cos\alpha_2 + (Q_2-Q_1)\tan\phi_v \tag{6.42}$$

Summing the forces parallel to the bedding plane, the Q_2 force can be calculated as shown below:

$$Q_2 = Q_1 + N_2\tan\phi_h + (W_2+P_2)\sin\alpha_2 \qquad (6.43)$$

Substituting for N_2 and rearranging gives:

$$Q_2 = Q_1 + \frac{(W_2 + P_2)(\sin\alpha_2 + \tan\phi_h\cos\alpha_2)}{1 - \tan\phi_h \tan\phi_v} \qquad (6.44)$$

For general forces Ni and Q_n, it can be proven that:

$$N_i = (W_i+P_i)\cos\alpha_i + (Q_i-Q_{i-1})\tan\phi_v \qquad (6.45)$$

and

$$Q_n = \sum_{i=1}^{n} \frac{(W_i + P_i)(\sin\alpha_i + \tan\phi_h\cos\alpha_i)}{1 - \tan\phi_h \tan\phi_v} \qquad (6.46)$$

The computational codes to solve Q force Equations derived in Section 6.4 for various slope shapes are given in the Appendix, Section A2.

6.5 COMPUTATIONAL MODEL USING UDEC

The model was used to study interactive forces between the block surfaces and to compare them with the forces derived when using analytical equations. Using the Universal Distinct Element Code UDEC (Itasca, 1993), the model was constructed to represent a fractured floor consisting of interacting blocks sliding on an inclined bedding plane. The free standing blocks used to model the fractured floor were 1m wide 2m high, while the base on which the blocks were sliding represented a failed horizontal bedding plane. To simulate an increase in floor elevation, the bedding was moved upwards at a predetermined rate. The floor was either a planar slope or curved into a parabolic shape as shown earlier in Figure 6.4. The blocks were gravity loaded and a vertical load of 650 tonne was applied onto the 4^{th}, 5^{th} and 6^{th} block from the face, to simulate the pressure induced by powered supports onto the floor. The "face block" shown on the left hand side of Figure 6.2 was fixed, to provide reaction forces to the moving blocks. The properties of fractured surfaces used in the numerical model are given in Table 6.1 (Nguyen, 1981), and the interacting forces between the block surfaces were studied. The computational code used here is given in the Appendix, Section A3.

Table 6.1 Rock and Fracture Properties used in UDEC Model (Nguyen, 1981)

	Bulk Modulus (GPa)	Shear Modulus (GPa)	Normal Stiffness (GPa)/m	Shear Stiffness (GPa)/m	Angle of Friction along Fractures	Cohesion (MPa)
Block Properties	9	6.7				
Bedding Fractures			9	6.7	15-35°	0
Vertical Fractures			9	6.7	15-45°	0

6.6 COMPARISON OF ANALYTICAL AND NUMERICAL SOLUTIONS

The possible cases of sliding models described earlier have been numerically modelled using UDEC, as shown in Figure 6.4. The analytical predictions for "Q-forces" represented by Equations 6.23, 6.24, 6.28, 6.38 and 6.46 are compared with UDEC numerical results for block rotation and no rotation.

6.6.1 Moving Blocks standing on Inclined Planar Bedding Surface

Moving blocks modelled on the inclined planar bedding surface experienced slip along the vertical and horizontal fractures, without rotation. Calculated and modelled Q forces are compared in Figure 6.5 where, for low angles of friction along the fractures, the modelled Q force approximates the calculated force from Equation 6.23 that describes the "no rotation" movement. When angles of friction were greater than 25° the interacting Q force appears to follow a lower path than the calculated force of non-rotating blocks. Reduction of the expected Q force in the model reflects the complex movement of all six modelled blocks, where some blocks were displaced along the fractures only, whilst others were rotated slightly. Magnified displacements from the UDEC model of blocks with no rotation are shown in Figure 6.4a, while slip along the bedding plane with no vertical slip, is shown in Figure 6.4b. Block movement conditions modelled by UDEC were magnified for clarity.

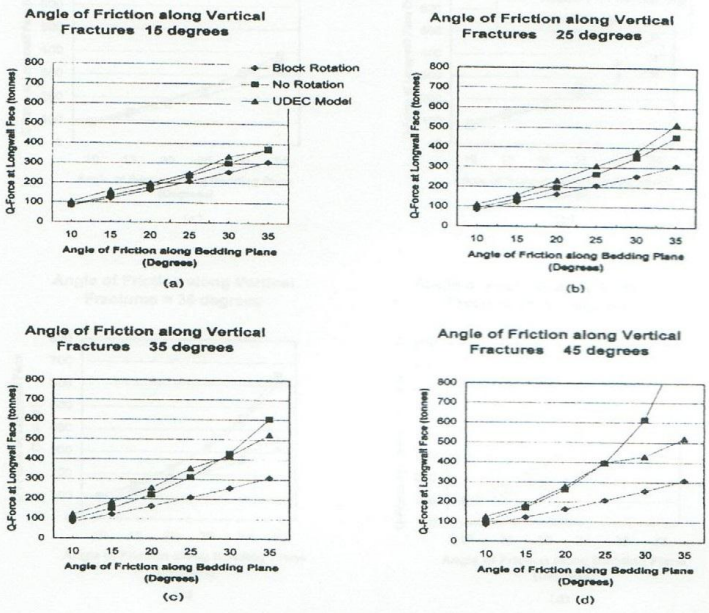

Figure 6.5 Interacting Q force between floor blocks standing on moving planar bedding plane

6.6.2 Moving Blocks standing on Curved Bedding Surface

When modelling the parabolic inclination of floor taking the shape of curve $y = x^2/400$, the blocks were approximating the rotations shown in Figure 6.4(c). The Q forces obtained from the model were compared to the forces derived by Equations 6.24, 6.38 and 6.46, and are shown in Figure 6.6.

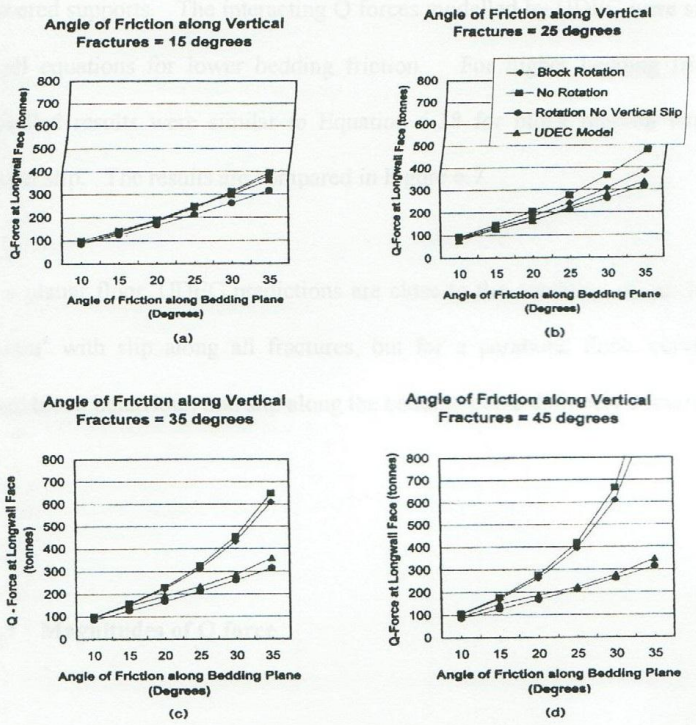

Figure 6.6 Interacting Q force between floor blocks standing on moving curved bedding plane of shape $x^2/400$

The above plots indicate that for the described geometry the modelled Q forces were slightly smaller than calculated Q forces.

When the floor was inclined in the shape of $y = x^2/200$, upward movement of the modelled floor induced block displacement similar to the previous case. The magnified UDEC displacements shown in Figure 6.4c indicated that the blocks rotated and slipped along the bedding plane but did not slip along the

vertical fractures. The exceptions were blocks 1 and 2, which were loaded by powered supports. The interacting Q forces modelled by UDEC were similar to all equations for lower bedding friction. For higher bedding friction, modelled results were similar to Equation 6.38 for block rotation with no vertical slip. The results are compared in Figure 6.7.

For a planar floor, UDEC predictions are close to the condition of 'no block rotation' with slip along all fractures, but for a parabolic floor, curvature varied block behaviour, and slip along the bedding plane definitely occurred.

6.6.3 Magnitudes of Q force

The Q force magnitude acting at the block corners increased with the angle of friction along the bedding plane, and also increased with the angle of friction along the vertical fractures in all cases where movement along these fractures occurred. Figure 6.5 shown that for a given geometry and a low angle of friction equal to 10°, the Q force was approximately 1000kN (100 tonnes) for all calculated and modelled cases. As the angle of friction along the bedding plane increased to 30°, the modelled Q force in the planar floor model varied from 3400kN to 4300kN (340-430 tonnes) depending on the angle of friction along the vertical fractures. When compared to the analytical equations the Q force varied from 2600kN (260 tonnes) for a 'block rotation' condition to a maximum of 6100kN (610 tonnes) for a 'no block rotation' condition. As

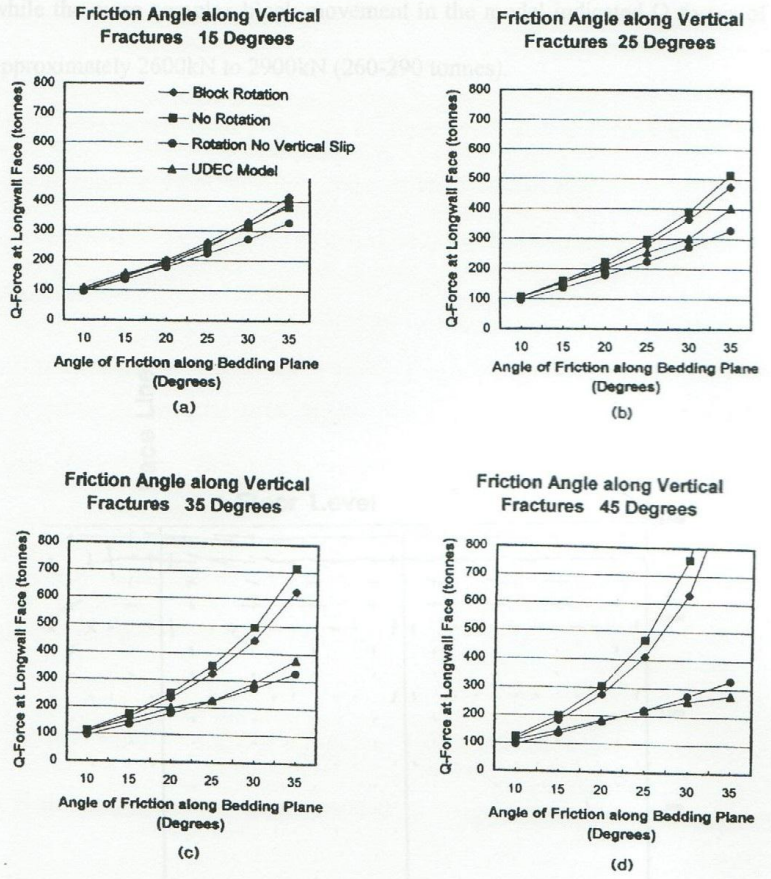

Figure 6.7 Interacting Q force between floor blocks standing on moving curved bedding plane of shape $x^2/200$

expected, Q forces for the parabolic floor inclination were independent of the friction angle along the vertical fractures, where slip did not occur. For the 30° of friction angle of along the bedding plane, calculated Q forces on the curved plane varied from approximately 3000kN to 4600kN (300-460 tonnes),

while the more complex block movement in the model indicated Q forces of approximately 2600kN to 2900kN (260-290 tonnes).

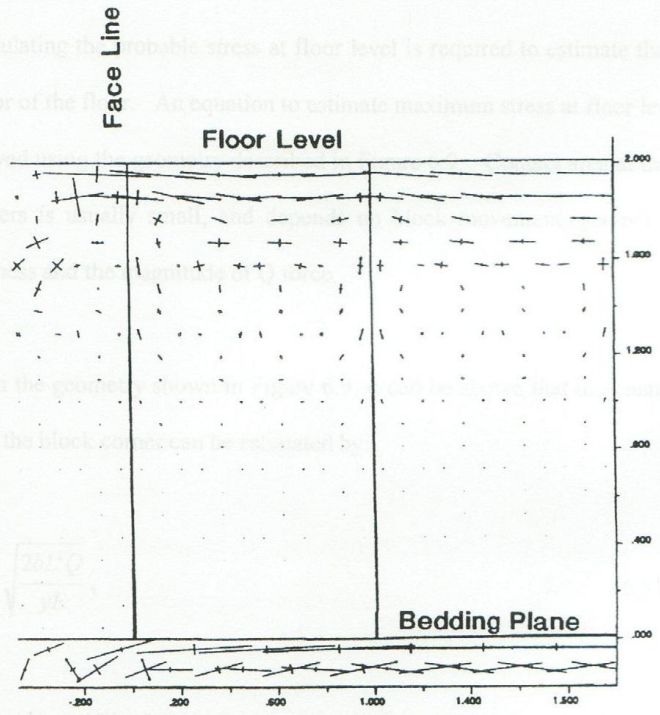

Figure 6.8 UDEC model showing concentrations of lateral stress at floor level

6.7 STRESS AT FLOOR LEVEL

Block interactions occur typically at floor level and as expected, lateral stresses concentrate in the upper edges of the blocks at floor level. Typical concentrations of lateral stress at floor level modelled by UDEC are shown in Figure 6.8.

Calculating the probable stress at floor level is required to estimate the safety factor of the floor. An equation to estimate maximum stress at floor level was derived using the geometry described in Figure 6.9. Contact area at the block corners is usually small, and depends on block movement, geometry, rock stiffness and the magnitude of Q force.

From the geometry shown in Figure 6.9, it can be shown that the contact area A at the block corner can be estimated by:

$$A = \sqrt{\frac{2bL^2Q}{yE}}, \qquad (6.51)$$

where: b = width of the block along the face equal of the width of the powered support,

L = width of the block at perpendicular to the face,

Q = interacting force at block corner,

y = floor lift, and

E = Young's modulus

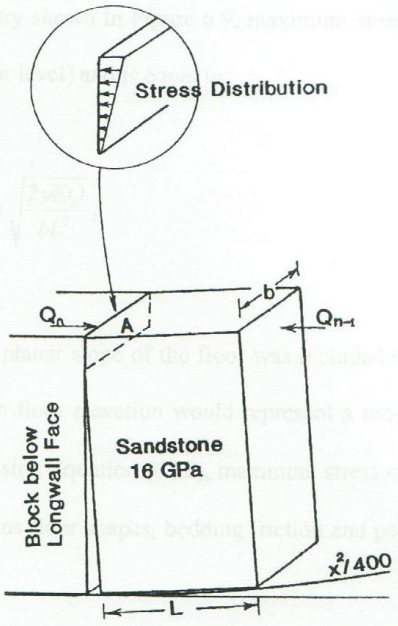

Figure 6.9 Area of contact between blocks in the floor

Calculations of the contact area between the blocks using Equation (6.51) are within 10% of the contact area observed in the UDEC model.

The average stress at the contact area can be calculated using:

$$\sigma_{\text{average}} = \frac{Q}{A} = \sqrt{\frac{yEQ}{2bL^2}}, \tag{6.52}$$

From the geometry shown in Figure 6.9, maximum stress develops at the top of the block (floor level) and is equal to:

$$\sigma_{max} = 2\sigma_{average} = \sqrt{\frac{2yEQ}{bL^2}}, \qquad (6.53)$$

Even though the planar slope of the floor was included in the study, the non-planar increase in floor elevation would represent a more realistic behaviour (Peng, 1984). Using Equation (6.53), maximum stress σ_{max} was calculated at the face for various floor shapes, bedding friction and powered support loads. These were:

Floor curvature:	$y=x^2/400$, $y=x^2/200$, $y=x^2/100$ and $y=x^2/50$
Friction angle of floor	10°, 15°, 20°, 25°, 30° and 35°
Powered support load	400, 500, 600, 700, 800 and 900 tonnes

The increase in slope, bedding friction and powered support loads appeared to have a significant influence on the magnitude of calculated stress σ_{max}. A reduction of contact area at the block corners and an increase of the Q force was experienced when floor curvature changed from $y = x^2/400$ to $y = x^2/50$.

The calculated floor stress levels presented in Figures 6.10 and 6.11 indicate a wide variety of possible stresses at floor level. For friction angles along the bedding plane varying from 10° to 15°, and for low floor curvature ($y = x^2/400$) maximum floor stress varied from approximately 6 to 10 MPa

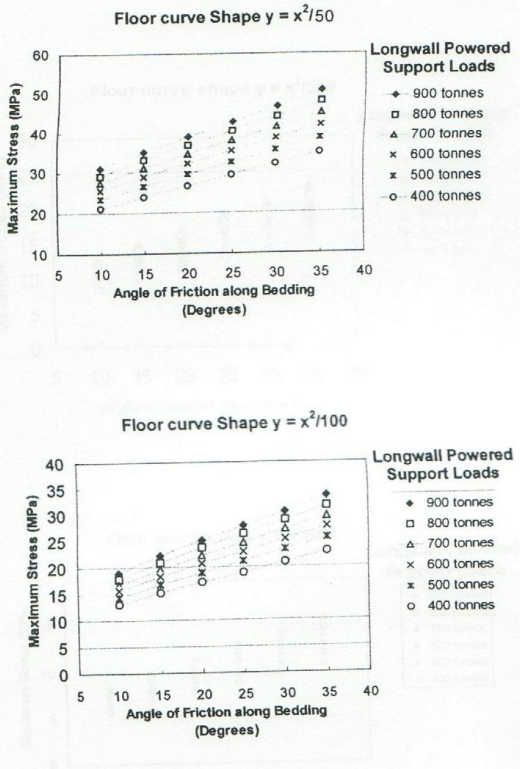

Figure 6.10 Calculated maximum lateral stress at floor level for $y=x^2/50$ and $y=x^2/100$

depending on the load below the powered supports. For steeper floor curvature approaching $y = x^2/50$ and larger angles of friction (ϕ=30° to 35°), stress magnitudes increased dramatically, ranging between 32 and 50 MPa. These stress magnitudes are well within the range of the insitu strength of rocks typically found in coal mine floors (Karabin, 1999).

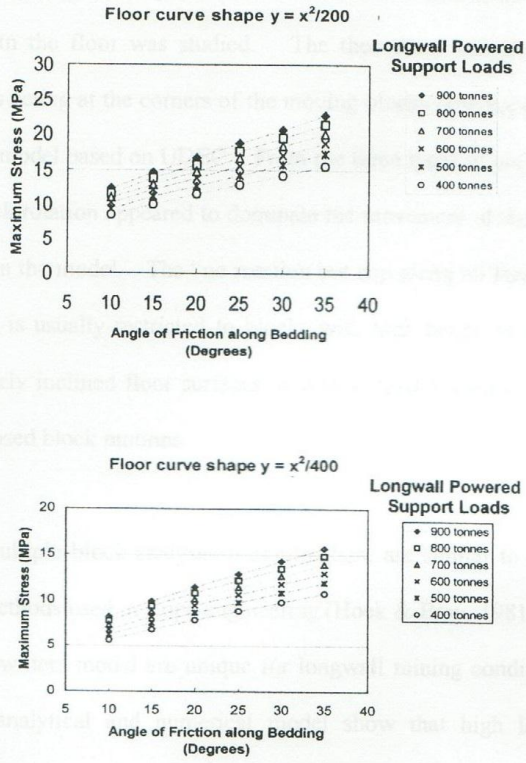

Figure 6.11 Calculated maximum lateral stress at floor level for $y=x^2/200$ and $y=x^2/400$

6.8 SUMMARY

The effect of moving blocks along fractured interfaces and its influence on stress distribution in the floor was studied. The theoretical solutions for interacting Q forces acting at the corners of the moving blocks compared well with the numerical model based on UDEC. From the three types of proposed block motions, block rotation appeared to dominate the movement of the non-planar floor shape in the model. The "no rotation but slip along all fractured surfaces" condition is usually restricted to blocks with high height to width ratios but for severely inclined floor surfaces, complex block movement can occur with all proposed block motions.

Even though the multiple block analyses presented here are similar to some limit equilibrium methods used in slope engineering (Hoek & Bray, 1981), the applications of the writers model are unique for longwall mining conditions. Results from the analytical and numerical model show that high lateral stresses can exist at the top of each moving block, and the magnitudes of interacting forces can be large enough to induce floor failure. The analytical solutions indicate that calculated interaction forces between the blocks increased with the distance towards the face, and as expected, stress transfer locations are usually at the unconfined floor level. The study indicated that maximum stresses at floor level increased mainly with (i) an increase in longwall support loads, (ii) the angle of friction along the bedding plane on which the blocks slide, and (iii) an increase in floor curvature.

The calculated and modelled contact area at the tip of each block appeared relatively small, allowing interacting lateral stress to exceed rock strength and induce rock failure at floor level. The block movement mechanism indicates that if floor failure occurs, it will begin at the surface and propagate lower down. The theoretical equations formulated in this study would give the practising mining or geotechnical engineer a useful tool for predicting floor stability at the longwall face. Even though the mechanism for moving blocks in the floor and the derived equations for interacting forces describe a new approach to analysing stress distribution in the immediate floor, further work is needed to fully assess the applications of this method.